Investigating Protein Structure Change in the Zona Pellucida with a Microrobotic System

Yu Sun, Bradley J. Nelson and Michael A. Greminger

The International Journal of Robotics Research 2005 24: 211
DOI: 10.1177/0278364905050360

Yu Sun
Bradley J. Nelson

Swiss Federal Institute of Technology
ETH Zurich, Switzerland
sun@iris.mavt.ethz.ch

Michael A. Greminger

University of Minnesota
Minnesota, USA

Investigating Protein Structure Change in the Zona Pellucida with a Microrobotic System

Abstract

In this paper we present a microrobotic system that integrates microscope vision and microforce feedback for characterizing biomembrane mechanical properties. We describe robust visual tracking of deformable biomembrane contours using physics-based models. A multi-axis microelectromechanical systems based force sensor is used to determine applied forces on biomembranes and to develop a novel biomembrane mechanical model. By visually extracting biomembrane deformations during loading, geometry changes can be used to estimate applied forces using a biomembrane mechanical model and the determined elastic modulus. Forces on a biomembrane can be visually observed and controlled, thus creating a framework for vision and force assimilated cell manipulation. The experimental results quantitatively describe a stiffness increase seen in the mouse zona pellucida (ZP) after fertilization. Understanding this stiffness increase, referred to as "zona hardening", helps provide an understanding of ZP protein structure development, i.e., an increase in the number of cross links of protein ZP1 between ZP2 and ZP3 units that is conjectured to be responsible for zona hardening. Furthermore, the system, technique, and model presented in this paper can be applied to investigating mechanical properties of other biomembranes and other cell types, which has the potential to facilitate many biological studies, such as cell injury and recovery where biomembrane mechanical property changes need to be monitored.

KEY WORDS—zona pellucida proteins, protein cross-linking, stiffness, microrobotic cell manipulation, microelectromechanical systems, boundary element, deformable visual tracking, vision-based force sensing

1. Introduction

Biomembranes isolate biological cells from their immediate surroundings and can play a key role in modulating the transport of substances between the cell and its environment. Investigations into the functions and behaviors of various cells often require that their corresponding biomembranes are characterized. The most common biomembranes are composed of lipids and proteins, such as plasma membranes. Membrane lipids are organized in a bilayer that has two closely opposed sheets. Embedded in and associated with the lipid portion of the membrane are proteins. There are other types of biomembranes that have compositions different than lipid bilayer membranes. The zona pellucida (ZP) is an extracellular biomembrane enveloping an oocyte. It is composed of three sulfated glycoproteins, called ZP1, ZP2 and ZP3 that are synthesized by the oocyte (Liang et al. 1995).

In this paper, an understanding of the protein structure in ZP is pursued through ZP mechanical property characterization using a microrobotic system integrating vision and force feedback. Upon fertilization, the ZP surrounding the oocyte undergoes a "hardening" process in order to prevent subsequent spermatozoon from penetrating. To better understand the mechanical properties of ZP and the mechanical property changes during zona hardening, biomembrane mechanical property characterization is conducted on mouse oocytes and embryos.

A microrobotic system with biomembrane force sensing capabilities is described in this paper. A deformable cell membrane contour tracking algorithm using physics-based models is presented. Using the visual tracking information, vision-based biomembrane force estimation strategy is investigated. Robust tracking of cell deformation is shown, and real-time determination of applied force fields is demonstrated. The experimental results quantitatively describe the mechanical properties of mouse oocyte and embryo ZP. These results help justify speculation that an increase in the number of cross

The International Journal of Robotics Research
Vol. 24, No. 2–3, February–March 2005, pp. 211-218,
DOI: 10.1177/0278364905050360

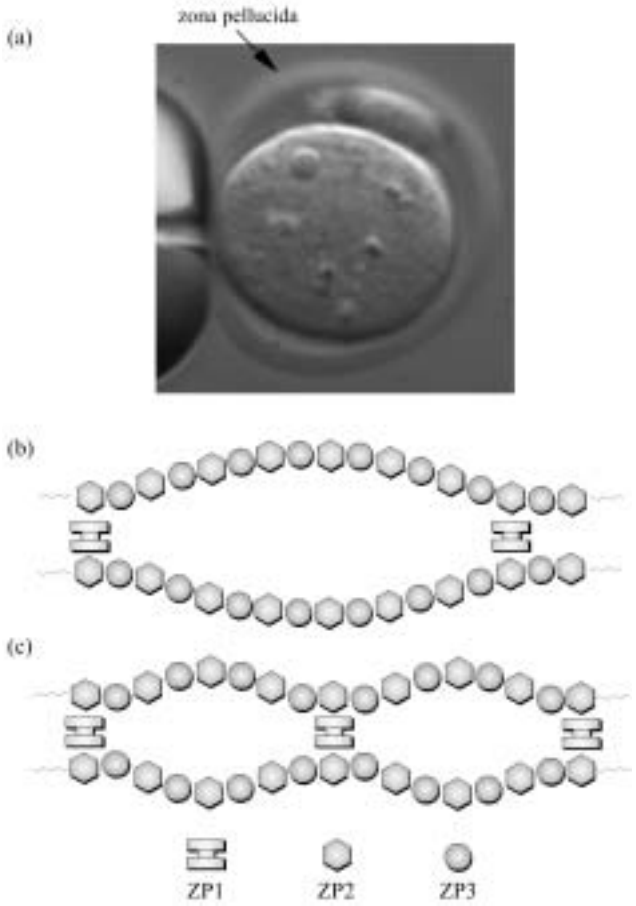

Fig. 1. ZP and its protein structure: (a) ZP membrane enveloping a mouse embryo; (b) protein structure before fertilization (redrawn from Green 1997); (c) after fertilization. The increase of ZP1 cross-links is speculated to cause zona hardening.

links of protein ZP1 between ZP2 and ZP3 units is responsible for the observed ZP stiffness increase observed during zona hardening (Green 1997). This cross-linking is shown schematically in Figure 1.

Furthermore, the system, technique, and model presented in this paper can be applied to mechanical property investigations of other biomembranes and other cell types.

2. Microrobotic System for Characterizing Biomembrane Mechanical Properties

The microrobotic system is composed of two three-degrees-of-freedom (3-DOF) microrobots for cell holding and manipulation, a capacitive cellular force sensor mounted on the manipulation microrobot, a vacuum unit, and a cell membrane

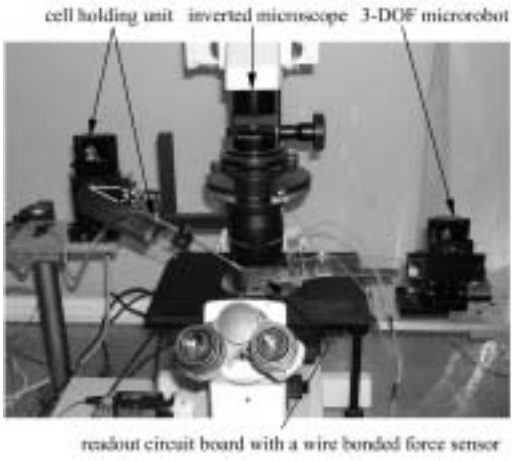

Fig. 2. Microrobotic system with vision and force feedback for biomembrane mechanical property characterization.

contour visual tracking unit, as shown in Figure 2. The microrobots have a travel of 2.54 cm with a step resolution of 40 nm in the xyz axes.

2.1. Microelectromechanical Systems Based Multi-Axis Capacitive Cellular Force Sensor

The microelectromechanical systems (MEMS) based two-axis cellular force sensor (Sun et al. 2002) shown in Figure 3 is capable of resolving normal forces applied to a cell as well as tangential forces generated by improperly aligned cell probes. A high-yield microfabrication process was developed to form the three-dimensional (3D) high aspect ratio structure by using deep reactive ion etching (DRIE) on silicon-on-insulator (SOI) wafers.

The constrained outer frame and the inner movable structure are connected by four curved springs. A load applied on the probe causes the inner structure to move, changing the gap between each pair of interdigitated comb capacitors. Consequently, the total capacitance change resolves the applied force. The interdigitated capacitors are orthogonally configured to make the force sensor capable of resolving forces in both the x- and y-direction. The cellular force sensors used in the experiments are capable of resolving forces up to 25 μN with a resolution as low as 0.01 μN.

Tip geometry effects the quantitative force measurement results. A standard injection pipette (Cook K-MPIP-1000-5) tip section with a tip diameter of 5 μm is attached to the probe of the cellular force sensors.

2.2. Visually Tracking Cell Deformation Using Physics-Based Models

In order to establish the quantitative relationships between applied forces and biomembrane geometry deformations so

Fig. 3. A cellular force sensor with orthogonal comb drives detailed.

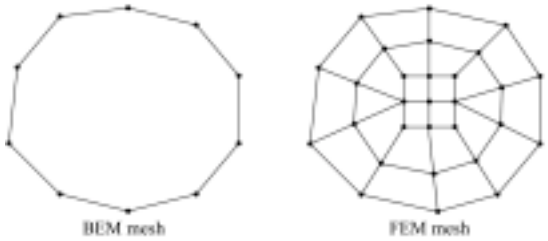

Fig. 4. Comparison between 2D boundary element and finite element meshes.

that biomembrane mechanical properties can be determined, a robust deformable visual tracking algorithm is required. Gradient-based tracking algorithms such as Snakes (Kass, Witkin, and Terzopoulos 1987) were not able to provide robust tracking performance in the experiments. One of the reasons is that the free-form algorithm has the generality that allows it to be used with a wide variety of object shapes. However, this generality also makes the gradient-based algorithm susceptible to noise and local minima since no assumptions are made about the object shape being tracked or its material properties.

2.2.1. Boundary Element Method

The boundary element method (BEM) provides a particularly well-formulated approach to physics-based modeling of object deformations based on object contours. Like the finite element method (FEM), the BEM is a technique to model an elastic solid. The BEM differs from the FEM in that only the contour of an object needs to be meshed, as illustrated by the different meshing techniques in Figure 4, making this method attractive for computer vision problems and especially for tracking object deformations.

When tracking a two-dimensional (2D) cross-section of a biological cell, it is apparent that the cell membrane deforms in a manner that can be approximated assuming 2D plane stress elasticity, despite the fact that biological cells are clearly not linearly elastic solids and cannot be precisely modeled as such. This assumption of linear elasticity provides robust constraints on the visual tracking algorithm and ensures that the extracted contour properly mimics the underlying physics of the cell deformation. The 2D plane stress elasticity problem can be expressed in terms of displacements $u(x)$ by (Sokolnikoff 1983)

$$\mu \nabla^2 u_\alpha + \mu \left(\frac{1+\nu}{1-\nu} \right) \frac{\partial}{\partial x_\alpha} \left(\frac{\partial u_1}{\partial x_1} + \frac{\partial u_2}{\partial x_2} \right) + F_\alpha = 0, \quad (1)$$

where $\alpha = 1, 2$. $F(x)$ is the body force applied to the object, such as gravity or a force due to acceleration. This equation is known as Navier's equation of plane stress and is defined over a 2D domain R with a boundary ∂R. The shear modulus μ and Poisson's ratio ν completely define the material properties of an isotropic linearly elastic object.

The boundary conditions for eq. (1) can be expressed as a prescribed traction vector $\{t\}$ over the boundary ∂R where, in two dimensions, the traction vector has the units of force per length. This is known as the Neumann problem. Solving the Neumann problem using the BEM method returns the nodal displacements $\{u\}$ which result from the applied tractions.

Once the nodal displacements $\{u\}$ are found by solving the Neumann problem, the displacement at any point on the boundary can be found by using quadratic interpolation (Beer 2001). The displacement at any point in the interior of the object can be found using Somigliana's identity (Rizzo 1967).

In order to track deformable objects, a deformable template is defined that uses the BEM to model displacements. The template is registered to the image by applying a force field that deforms the template to match the image. This force field is found using an energy minimization approach.

2.2.2. BEM Visual Tracking

The deformable template is registered to a binary edge image using a least-squares error measure. The template is represented by a list of 2D vertices r_i and the edge pixels in the current image are represented by the list of 2D vertices w_i. The registration algorithm minimizes the distance squared between the transformed template vertices r'_i and the nearest image edge vertices w_i, where the template vertices are transformed by an elastic transformation and a rigid body transformation.

The rigid body portion of the transformation of the template vertices is simply an affine transformation given by

$$r'_i = A(r_i) \quad (2)$$

where A is defined by

$$A(r_i) = X + \begin{bmatrix} \cos\theta & -\sin\theta \\ \sin\theta & \cos\theta \end{bmatrix} r_i. \quad (3)$$

Here, θ is the angle of rotation and X is the translation vector. The error function between the transformed template vertices

r_i' and the image vertices w_i can be written as

$$E(\theta, X) = \sum_{j=1}^{M} \left\| r_j' - w_j \right\|^2, \tag{4}$$

where r_j' is the position vector of the ith edge pixel of the template transformed by eq. (2), w_j is the position vector of the edge pixel in the image that is closest to the point r_j', and M is the number of edge pixels in the template. This error function sums the square of the distance between each template vertex and the nearest image edge pixel. Since the transformed template vertices r_j' are transformed by the affine transform A, E will be a function of θ and X. By minimizing E, the values of θ and X that best match in the image in a least-squares sense will be found. The error function E is minimized by a gradient-based multivariable minimization technique called the Broydon–Fletcher–Goldfarb–Shanno method (Vanderplaats 1984).

Minimizing eq. (4) will determine the rigid body motion of the object. The BEM will be used to model the non-rigid portion of the objects motion. To do this, the template is deformed according to the BEM model before performing the affine transformation. The transformation becomes

$$r_i' = A\,(r_i + u(r_i, \{t\})) \tag{5}$$

where $u(r_i, \{t\})$ is the displacement of the template edge pixel r_i due to the applied traction distribution $\{t\}$ on the boundary of the object. The displacement vector $u(r_i, \{t\})$ is obtained from the solution to the Neumann problem. The error function (4) becomes

$$E(\theta, X, \{t\}) = \sum_{i=1}^{M} \left\| r_i' - w_i \right\|^2. \tag{6}$$

Since the error function (6) has an additional parameter $\{t\}$, minimizing the error function will now give the traction distribution $\{t\}$ in addition to the position and orientation of the object. This algorithm tracks the deformable object by finding the traction distribution $\{t\}$ that, when applied to the template, causes the template to match the image.

Robust tracking of cell deformation has been achieved. The results of the BEM template matching algorithm applied to cell contour tracking are shown in Figure 5, where the traction distribution applied to the template is shown on the right.

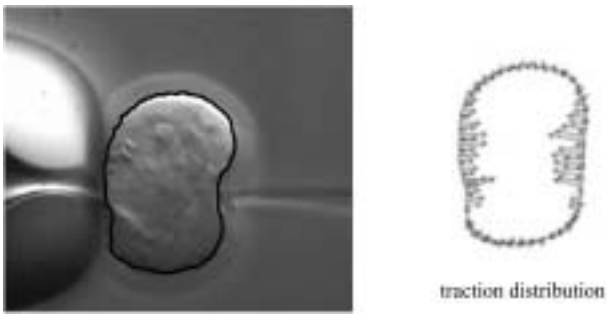

Fig. 5. Visual tracking of a deformed cell contour and the traction distribution $\{t\}$ applied to template used to track the contour.

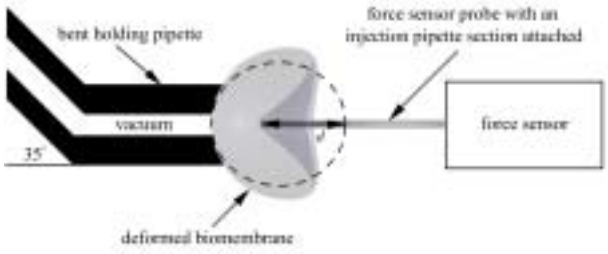

Fig. 6. Force–distance measurement system configuration (not to scale).

2.3. Experimental Results

Mouse oocytes and embryos used in the experiments were collected in accordance with standard established procedures (Hogan et al. 1994). The system configuration under the microscope is shown in Figure 6. The bent holding pipette tip, the cell, and the force sensor probe are horizontally aligned.

Before the force sensor applied a uniaxial point load compressing the biomembrane and measured normal forces, the force sensor probe was aligned such that tangential forces were minimized to ensure that only a normal force was applied to the membrane.

Figure 7 shows the force and deformation measurement process. As shown in Figure 8, forces increase nonlinearly as deformation increases. For mouse oocytes, when deformation reaches about 45 μm, the ZP and the plasma membrane are punctured, which results in the maximum forces measured, i.e., the puncturing forces. The puncturing forces are approximately 7.5 μN. After the force sensor tip punctures the membranes and travels into the cytoplasm, the force decreases rapidly, almost to zero.

It can be seen that embryo membranes endure much larger deformations than oocyte membranes before being punctured. The required forces to puncture embryo membranes are almost twice as large as the forces for oocyte membranes. These measurement results quantitatively reveal the mechanical property differences that result from mouse ZP hardening and illustrate differences in manipulating cells of different types and different stages of development. In order to understand how cell deformation properties change, it is necessary to relate visually observed cell deformations to measured forces. This requires a biomembrane mechanical model.

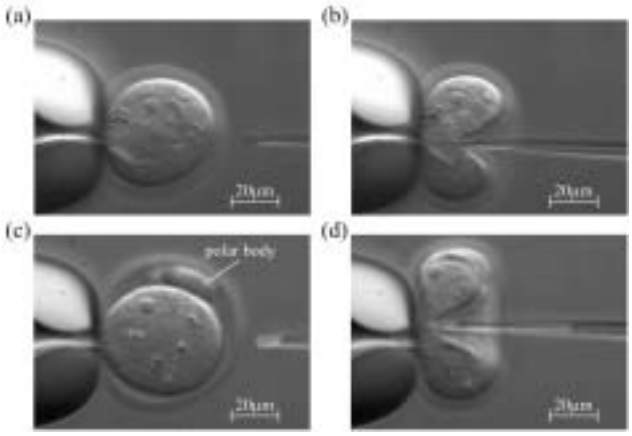

Fig. 7. Force–displacement curve measurement: (a), (b) mouse oocyte ZP (applied force, 7.21 μN; indenter displacement, 42.2 μm); (c), (d) mouse embryo ZP (applied force, 12.7 μN; indenter displacement, 52.3 μm).

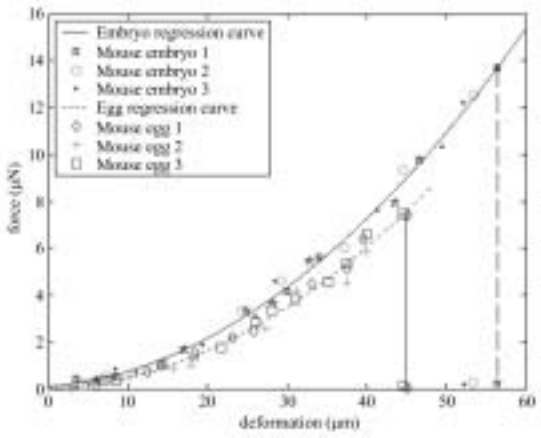

Fig. 8. Force–deformation curves of mouse oocyte and embryo membranes.

3. Biomembrane Mechanical Modeling

Although the assumption of 2D plane stress elasticity was useful for constraining the contour extraction algorithm for measuring cell membrane deformation as described in Section 2.3, this assumption is poor for determining realistic material parameters of the ZP, such as the modulus of elasticity. Instead, a biomembrane mechanical model that more accurately describes the actual loading and material conditions is required.

The two popular biocapsule models are the contact mechanics models and the micropipette aspiration model. The contact mechanics models, including the Hertzian model (Johnson 1987) and Sneddon model (Maugis 2000), treat a deformed object as a solid body; however, encapsulated biocapsules are by no means solid bodies. The micropipette aspiration model (Evans and Shalak 1980) assumes that a sucking pressure is applied to deform a biomembrane while uniaxial forces are applied on the mouse cell membranes in our experiments. Thus, these existing models do not apply in describing the mouse oocyte and embryo membrane loading situations.

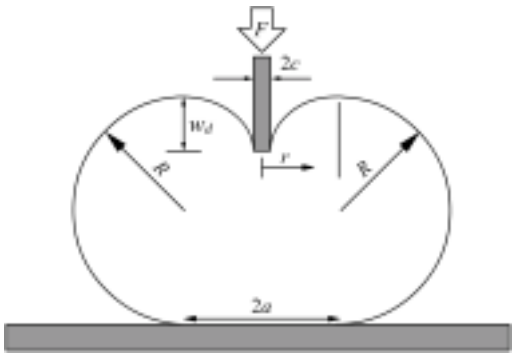

Fig. 9. Indentation of a cell membrane by a micropipette.

3.1. Biomembrane Point-Load Model

Due to the deficiencies of existing models, a new biomembrane point-load model is developed, which considers a biomembrane as a thin film and assumes that the inner cytoplasm provides a hydrostatic pressure on the membrane. The model assumptions include: (a) the biomembrane encapsulates liquid (i.e., cytoplasm) that exerts a uniform hydrostatic pressure on the biomembrane; (b) the cell volume does not change; (c) the biomembrane has a negligible flexural rigidity, so that deformation is caused by membrane stretching alone; (d) the biomembrane is linearly elastic; (e) the cell is free of initial membrane stress or residual stress; (f) the model starts with a planar circular area with zero residual stress.

From experimental observations, an indented biomembrane shape can be characterized with three geometric parameters a, w_d and R, as shown in Figure 9. A micropipette of radius c exerts a force F on the membrane, creating a dimple with radius a and depth w_d and semicircular curved surfaces with radius R.

In deriving the model, first consider force equilibrium at the local dimple. As shown in Figure 10, the internal pressure produces a force $\pi r^2 p$ counterbalancing the applied force F, where p is the internal pressure. Another counterbalancing force, $\sigma_d \sin\theta 2\pi r h$ is due to the membrane stress σ_d. These two forces together balance the applied force F. For small-angle approximations, $\mathrm{d}w/\mathrm{d}r \approx \sin\theta \approx \theta$, where w is the deformed dimple profile (Wan, Chan, and Dillard 2002). Thus,

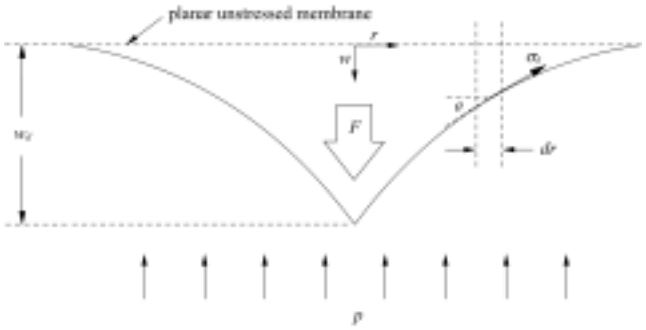

Fig. 10. Force balance and elastic strain analysis at the dimple.

the force balance equation at equilibrium is

$$F = \pi r^2 p + \sigma_d 2\pi r h \frac{\mathrm{d}w}{\mathrm{d}r}$$

or

$$\sigma_d h \frac{\mathrm{d}w}{\mathrm{d}r} = \frac{F}{2\pi r} - \frac{pr}{2}, \tag{7}$$

where h is membrane thickness.

Integrating eq. (7) with a boundary condition of $w = 0$ at $r = a$ and approximating $p = F/(\pi a^2)$ yield the dimple profile

$$w = -\frac{F}{4\pi\sigma_d h}\left[1 - \left(\frac{r}{a}\right)^2 + \ln\left(\frac{r}{a}\right)^2\right], \tag{8}$$

which is valid in $c \le r \le a$.

The dimple depth from the maximum height of the deformed membrane, as shown in Figure 9, is given by

$$w_d = w\big|_{r=c} = -\frac{F}{4\pi\sigma_d h}\left[1 - \left(\frac{c}{a}\right)^2 + \ln\left(\frac{c}{a}\right)^2\right]. \tag{9}$$

Within the dimple, each ring element on the membrane of radius r and width $\mathrm{d}r$ is stretched by the external load to a final width of $\mathrm{d}r/\cos\theta$, as shown in Figure 10. If $\theta < 25^\circ$ holds, the small strain approximation is valid. The largest θ in the experiments is less than 22°. The elastic strain on such an element is, therefore, given by

$$\begin{aligned}\varepsilon_d &= \frac{\mathrm{d}r/\cos\theta - \mathrm{d}r}{\mathrm{d}r} \approx \frac{\theta^2}{2} \\ &= \frac{1}{2}\left(\frac{\mathrm{d}w}{\mathrm{d}r}\right)^2.\end{aligned} \tag{10}$$

Since elastic strain on a membrane is proportional to area change (Wan, Chan, and Dillard 2002), one can ignore the second-order terms, and the average strain on the membrane is

$$\bar{\varepsilon}_d = \frac{1}{2}\frac{\int_c^a (1/2)\,(\mathrm{d}w/\mathrm{d}r)^2\, r\,\mathrm{d}r}{\int_c^a r\,\mathrm{d}r}. \tag{11}$$

Note that the denominator is simply the area of the annulus, with c and a the inner and outer radii, respectively.

Linear elasticity requires (Dietrich, Angelova, and Pouligny 1997; Wan and Liu 2001)

$$\bar{\sigma}_d = \frac{E}{1-\nu}\bar{\varepsilon}_d, \tag{12}$$

where E is the membrane elastic modulus and ν is Poisson's ratio.

Combining eqs. (9) and (12) yields

$$F = \frac{2\pi E h w_d^3}{a^2(1-\nu)}\left[\frac{3 - 4\zeta^2 + \zeta^4 + 2\ln\zeta^2}{(1-\zeta^2)(1-\zeta^2+\ln\zeta^2)^3}\right], \tag{13}$$

where $\zeta = c/a$.

3.2. Determination of Mouse ZP Elastic Modulus

The geometric parameters a and w_d are extracted from the deformable tracking algorithm. F is the measured force. The Poisson ratio ν of biomembranes is typically assumed to be 0.5. The constant values used are 4.5 μm in ZP thickness (h) and 3 μm in indenter radius (c). Using eq. (13) of the biomembrane point-load model, the Young's moduli of mouse oocyte and embryo ZP are calculated.

Table 1 summarizes the elastic modulus results, based on 34 data points from three mouse oocytes and 31 data points from three mouse embryos. Throughout the ZP loading process, the modulus values are fairly constant.

4. Vision-Based Biomembrane Force Estimation

When vision and force measurements are integrated, the elastic modulus of a biomembrane can be determined from the force and visual feedback. Conversely, if the biomembrane elastic modulus is determined, applied forces can be estimated from visual feedback alone, a technique referred to as vision-based biomembrane force sensing.

Figure 11 shows the vision-based biomembrane force estimation results on an oocyte ZP. The geometric parameters are extracted using the deformable template matching algorithm and the elastic modulus used in calculation is the mean value 17.9 kPa shown in Table 1. Consequently, applied forces are estimated from eq. (13). In Figure 11, the horizontal axis is

Table 1. Elastic Modulus of Mouse Oocyte and Embryo ZP

Statistics	Oocyte ZP Modulus (kPa)	Embryo ZP Modulus (kPa)
Mean	17.9	42.2
Standard deviation (1σ)	0.8	2.1

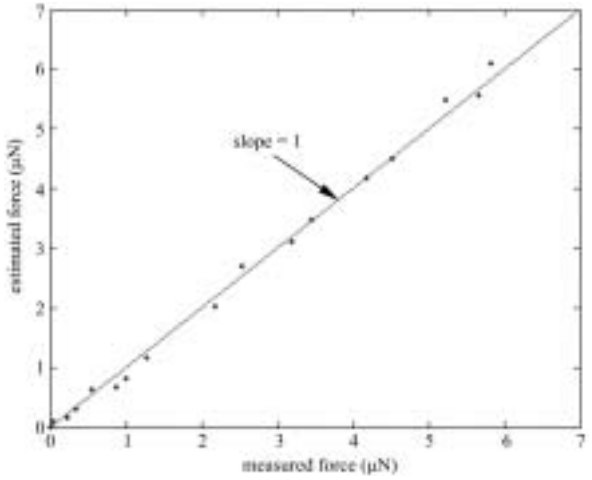

Fig. 11. Vision-based force estimation versus measured forces.

the measured force from the force sensor in the experiments. The vision-based biomembrane force estimation uncertainty is 0.389 μN (1σ), assuming zero measurement uncertainty for the measured force data on the horizontal axis.

5. Discussion

Historically, ZP hardening has a twofold meaning. One refers to the increased chemical resistance of ZP to proteolytic digestion, normally assessed with alpha-chymotrypsin (Demeestere, Barlow, and Leroy 1997). The second implication is an increase of ZP stiffness, which until now has been speculation without experimental proof. The experimental results presented in this paper quantitate the stiffness change during the ZP hardening process, which is a first in molecular biology. The significance of this research, however, goes beyond revealing the stiffness change.

The most widely accepted ZP structure model was proposed by Wassarman (1988). In this model, shown in Figure 1, protein ZP2 and ZP3 form filaments and are cross-linked by protein ZP1. Although ZP stiffness increase during ZP hardening has not been previously proven, it has been speculated that an increase of the number of cross-links of ZP1 between ZP2 and ZP3 units is responsible for a stiffness increase, if ZP stiffness increases at all. The experimental results in this paper quantitatively describe mouse ZP stiffness increase and help justify the previous speculation on ZP's protein structure change during ZP hardening, which provides an understanding of ZP protein structure development. It should be noted that reported results on other cell types, such as human foreskin fibroblasts and HeLa cells using the magnetic tweezers method (Bausch, Möller, and Sackmann 1999) revealed that protein cross-linking is also capable of inducing plasma membrane hardening (Xu, Tseng, and Wirtz 2000).

Other techniques that can be used for characterizing mouse ZP mechanical properties include the micropipette suction technique (Evans and Shalak 1980), the magnetic tweezers method (Bausch, Möller, and Sackmann 1999), and the atomic force microscopy (AFM) technique (Sato et al. 2000). Compared to other techniques, the technique presented in this paper is not only capable of measuring membrane forces but also suitable for manipulating biological cells with visual and force feedback. Furthermore, this technique uses an experimental setup and conditions consistent with intracytoplasmic sperm injection (ICSI), thus providing valid measurement results and information on ZP properties particularly relevant for ICSI studies.

The system, technique, and model presented in this paper can be applied to investigating the mechanical properties of other biomembranes and other cell types, which has the potential to facilitate many biological studies. For example, in cell injury and recovery studies, it is important to monitor biomembrane mechanical properties to detect membrane damage and to interpret such reported phenomenon as mechanical resistance to cellular volume reduction during dehydration and its relationship to injury.

6. Conclusions

In this paper we have presented a microrobotic system integrating microscope vision and microforce feedback for characterizing biomembrane mechanical properties. Robust visual tracking of deformable biomembrane contour using physics-based models has been described. A multi-axis MEMS-based force sensor was used to determine applied forces on biomembranes and to develop a novel biomembrane mechanical model. By visually extracting geometry changes on a biomembrane, geometry changes can be used to estimate applied forces using the biomembrane mechanical model and the determined elastic modulus. Forces on a biomembrane can be visually observed and controlled, thus creating a framework for vision and force assimilated cell manipulation. The experimental results quantitatively describe mouse ZP stiffness increase during zona hardening and provide an understanding of ZP protein structure development, i.e., an increase in the number of cross-links of protein ZP1 between ZP2 and ZP3 units that is conjectured to be responsible for ZP stiffness increase. Furthermore, the system, technique, and model presented in this paper can be applied to investigating mechanical properties of other biomembranes and other cell types, which has the potential to facilitate many biological studies, such as cell injury and recovery studies.

References

Bausch, A. R., Möller, W., and Sackmann, E. 1999. Measurement of local viscoelasticity and forces in living cells by magnetic tweezers. *Biophysics Journal* 76:573–579.

Beer, G. 2001. *Programming the Boundary Element Method*, Wiley, New York.

Demeestere, I., Barlow, P., and Leroy, F. 1997. Hardening of zona pellucida of mouse oocytes and embryos in vivo and in vitro. *International Journal of Fertility and Women's Medicine* 42(3):219–222.

Dietrich, C., Angelova, M., and Pouligny, B. 1997. Adhesion of latex spheres to giant phospholipid vesicles: statics and dynamics. *Journal de Physique II, France* 7:1651–1682.

Evans, E., and Skalak, R. 1980. *Mechanics and Thermodynamics of Biomembranes*, CRC Press, Boca Raton, FL.

Green, D. P. L. 1997. Three-dimensional structure of the zona pellucida. *Journal of Reproduction and Fertility* 2:147–156.

Hogan, B., Beddington, R., Costantini, F., and Lacey, E. 1994. *Manipulating the Mouse Embryo: A Laboratory Manual*, 2nd edition, Cold Spring Harbor Laboratory Press, New York.

Johnson, K. L. 1987. *Contact Mechanics*, Cambridge University Press, Cambridge.

Kass, J., Witkin, A., and Terzopoulos, D. 1987. Snakes: active contour models. *International Journal of Computer Vision* 1(4):321–331.

Liang, L. F., Familari, M., Moos, M. C., and Dean, J. 1995. Coordinate expression of the three zona pellucida genes during mouse oogenesis. *Development* 121:1947–1956.

Maugis, D. 2000. *Contact, Adhesion and Rupture of Elastic Solids*, Springer-Verlag, Berlin.

Rizzo, F. J. 1967. An integral equation approach to boundary value problems of classical elastostatics. *Quarterly Applied Mathematics* 25:83–95.

Sato, M., Nagayama, K., Kataoka, N., Sasaki, M., and Hane, K. 2000. Local mechanical properties measured by atomic force microscopy for cultured boving endothelial cells exposed to shear stress. *Journal of Biomechanics* 33:127–135.

Sokolnikoff, I. 1983. *Mathematical Theory of Elasticity*, Krieger Publishing, Malabar, FL.

Sun, Yu, Nelson, B. J., Potasek, D. P., and Enikov, E. 2002. A bulk microfabricated multi-axis capacitive cellular force sensor using transverse comb drives. *Journal of Micromechanics and Microengineering* 12(6):832–840.

Vanderplaats, G. 1984. *Numerical Optimization Techniques for Engineering Design*, McGraw-Hill, New York.

Wan, K. T., and Liu, K. K. 2001. Contact mechanics of a thin-walled capsule adhered onto a rigid planar substrate. *Medical and Biological Engineering and Computing* 39:605–608.

Wan, K. T., Chan, V., and Dillard, D. A. 2002. Constitutive equation for elastic indentation of a thin-walled biomimetic microcapsule by an atomic force microscope tip. *Colloids and Surfaces B: Biointerfaces* 27:241–248.

Wassarman, P. M. 1988. Zona pellucida glycoproteins. *Annual Review of Biochemistry* 57:415–442.

Xu, J., Tseng, Y., and Wirtz, D. 2000. Strain hardening of actin filament networks. *Journal of Biological Chemistry* 275(46):35,886–35,892.